Superfocusing modes of surface plasmon polaritons in conical geometry based on the quasi-separation of variables approach

2007 J. Phys. A: Math. Theor. 40 12479

(http://iopscience.iop.org/1751-8121/40/41/015)

IOP Publishing Journal of Physics A: Mathematical and Theoretical

J. Phys. A: Math. Theor. **40** (2007) 12479–12503 doi:10.1088/1751-8113/40/41/015

Superfocusing modes of surface plasmon polaritons in conical geometry based on the quasi-separation of variables approach

Kazuyoshi Kurihara[1], **Akira Otomo**[1], **Atsushi Syouji**[1], **Junichi Takahara**[2], **Koji Suzuki**[3] **and Shiyoshi Yokoyama**[1]

[1] Kobe Advanced ICT Research Center, National Institute of Information and Communications Technology (NICT), Kobe 651-2492, Japan
[2] Department of Systems Innovation, Graduate School of Engineering Science, Osaka University, Toyonaka 560-8531, Japan
[3] Department of Applied Chemistry, Faculty of Science and Technology, Keio University, Yokohama 223-8522, Japan

Received 31 January 2007, in final form 29 July 2007
Published 25 September 2007
Online at stacks.iop.org/JPhysA/40/12479

Abstract

Analytic solutions to the superfocusing modes of surface plasmon polaritons in a conical geometry are theoretically studied using an ingenious method called the quasi-separation of variables. This method can be used to look for fundamental solutions to the wave equation for a field that must satisfy boundary conditions at all points on the continuous surface of tapered geometries. The set of differential equations exclusively separated from the wave equation can be consistently solved in combination with perturbation methods. This paper presents the zeroth-order perturbation solution of conical superfocusing modes with azimuthal symmetry and graphically represents them in electric field-line patterns.

PACS numbers: 02.30.Mv, 41.20.Gz, 78.20.−e, 78.20.Bh

1. Introduction

Superfocusing of surface plasmon polaritons (SPPs) propagating toward tapered metal tips has recently become the focus of attention as a possible way of delivering electromagnetic radiation to the nanoscale and thereby causing an extraordinary enhancement of the electromagnetic field in nano-optics [1–3]. Superfocusing SPPs are a compound concept whereby propagating SPPs are gradually slowed down and stopped at the tapered tip where they accumulate as localized SPPs. The study of superfocusing SPPs in tapered metal structures is essentially equivalent to studying localized SPPs at tapered metal tips, which play a critical role in nano-optical applications such as high-resolution near-field optical microscopy [4], nanolithography [5, 6] and giant surface-enhanced Raman scattering [7–11].

In theoretical investigations on superfocusing SPPs [1, 12–16], the cone is a basic geometry [1, 12, 13] because the spherical coordinates system is easily applied and empirical correspondences are found in experimental scanning probe tips. Although the exact solution is still unknown, adiabatic approximate solutions [1, 17, 18] based on SPPs in a cylindrical geometry [19] have been used in numerous cases [1, 12, 13, 20, 21]. In conical geometry, numerical methods such as the finite-difference time-domain (FDTD) method [22] become increasingly ineffective in the superfocusing regions where the wave numbers of conical SPPs become larger closer to the apex of the cone. Theoretical improvements are needed in order to deal with superfocusing of SPPs.

Recently, Babadjanyan *et al* [12] gave an analytic solution to the superfocusing problem of conical SPPs at the apex point. In the spherical coordinates system, they applied the separation of variables approach to the wave equation for a magnetic field at the apex point of the cone. While it is possible to use the separation of variables for the solutions around the apex, it is very difficult to extend such solutions to the full cone. Indeed, their solution is restricted to the apex of the cone simply because it satisfies boundary conditions at only the apex. The difficulty lies in an uncountably infinite number of boundary conditions at all points on the continuous surface of the cone from the apex to an infinite distance from it, which cannot be satisfied by taking a linear combination of a countably infinite number of fundamental solutions based on the ordinary separation of variables; thus, it is necessary to find a new analytic method for solving the partial differential equations (PDEs) that will allow us to readily extend their analytic solution to the full cone. Generalized methods of the separation of variables [23–25] are worth considering.

The present paper proposes a new analytic method based on the quasi-separation of variables; it involves searching for fundamental solutions that each satisfy the boundary conditions on the continuous surface of tapered geometries, consequently making approximate analytic solutions to superfocusing SPPs more accurate than ever. Our solution in conical geometry includes the previous one by Babadjanyan *et al* [12] (see appendix A) and is a significant step toward findings exact solutions for the superfocusing modes of conical SPPs. In the method, solutions to the PDE in the superfocusing problem are assumed to be a product of functions depending on a common argument. As a result, it becomes possible to treat incomplete separated variables such as when the separation quantities are not fixed constants and depend on the common argument. For the superfocusing modes of conical SPPs in spherical coordinates, the magnetic field has only the azimuthal component, which is assumed to be multiplicatively separated into radial and polar angle functions depending on radius and both polar angle and radius, respectively. This assumption naturally leads to an incomplete separation of variables in such a manner that a separation quantity as a function of the 'radius' common argument is introduced in each of the metallic and dielectric regions to make the PDE exclusively separated into two differential equations: radial and extended polar angle equations. The radial equation becomes an ordinary differential equation (ODE) with respect to radius, which is considered for asymptotic boundary conditions at infinite and infinitesimal distances from the apex of the cone. The asymptotic behavior at infinity is treated as Sommerfeld's radiation condition [26] in which the wave number is set equal to that of the SPPs in planar geometry. According to both the asymptotic boundary conditions, the separation quantities that are differently expressed in metallic and dielectric regions become mathematically connected by a unified separation quantity independent of those regions. In contrast, the extended polar angle equation becomes a PDE with respect to two coordinates of polar angle and radius, which can be approximately solved using perturbation methods when it is regarded as an inhomogeneous ODE with respect to the polar angle. The inhomogeneous term is treated as a perturbation when the associated homogeneous ODE can be exactly solved.

Boundary conditions at the cone surface determine the unified separation quantity depending on the common argument of radius. A consistent theory of superfocusing SPPs based on the quasi-separation of variables in combination with perturbation methods is possible. In the present paper, the superfocusing modes of conical SPPs are considered in zeroth-order perturbation theory.

When the magnetic field has only the azimuthal component in spherical coordinates, it is easy to graphically represent the electric field-line patterns it induces. This graphical technique helps us to understand the analytic solutions of superfocusing SPPs visually and intuitively.

Finally, it is instructive to point out that the quasi-separation of variables is used in the Born–Oppenheimer adiabatic approximation [27, 28] for dividing the molecular wave function of quantum mechanics into two parts: the free nuclear motion described by a set of *slow* variables and the electric motion bound to the nuclei described by a set of *fast* variables together with a set of *slow* variables treated as fixed nuclear positions. In the Born–Oppenheimer approximation, the quasi-separation of variables is used to divide the total molecular system, as a consequence of the large ratio of nuclear mass to electron mass, into *slow* and *fast* subsystems of Hamiltonians that can be solved directly. This adiabatic concept in quantum theory cannot be applied in itself to the quasi-separation of variables in electromagnetic theory, which is introduced to express the strong coupling of superfocusing SPPs between the radius and polar angle in spherical coordinates without any specific condition such as the high ratio between nuclear and electric masses. For superfocusing problems in electromagnetic theory, we can exactly separate the original PDE of the Helmholtz wave equation into two sets of differential equations that can be solved mathematically by assuming just a quasi-separation of variables solution. When doing so, we do not need any knowledge of the Born–Oppenheimer adiabatic approximation, which is exactly the physical condition in quantum mechanics for allowing us to approximately separate a complex system into simpler subsystems by the quasi-separation of variables. Mathematical treatments due to the method are, however, fairly similar between quantum and electromagnetic theories, so that there exits a physical analogy indicated by the quasi-separation of variables: the complex system is separated into *slow* and *fast* subsystems. In superfocusing of conical SPPs, the radius and polar angle correspond to *slow* and *fast* variables, respectively; the radial and extended polar angle functions correspond to *slow* and *fast* subsystems, respectively. It may be of interest to note that the radial function of the *slow* subsystem describes the superfocusing effect in which the phase velocity becomes slower to zero as the conical tip is approached.

2. Quasi-separation of variables approach to the wave equation for a magnetic field

We employ a spherical system of coordinates (r, θ, φ) for the geometry of the conical structure in figure 1. The apex angle of the cone is 2α. The region of polar angle $0 < \theta < \alpha$ is occupied by a metallic cone with dielectric function ε_m while the outside of the cone is occupied by a dielectric material with dielectric function ε_d. Superfocusing modes in the conical structure are generally described as functions of spherical coordinates (r, θ, φ) and time t. We here consider a simple superfocusing mode of SPPs with azimuthal symmetry [29], whose magnetic field is directed along the φ-axis and depends only on r and θ [12]. The Maxwell equations for the magnetic field $\boldsymbol{H}(t)$ $(0, 0, H_\varphi(r, \theta, t))$ are simplified [12] to the scalar wave equation given by

$$\frac{1}{r}\frac{\partial^2}{\partial r^2} r H_\varphi(r,\theta) + \frac{1}{r^2}\frac{\partial}{\partial\theta}\frac{1}{\sin\theta}\frac{\partial}{\partial\theta} H_\varphi(r,\theta)\sin\theta + \varepsilon_j \frac{\omega^2}{c^2} H_\varphi(r,\theta) = 0, \qquad j = m, d \tag{1}$$

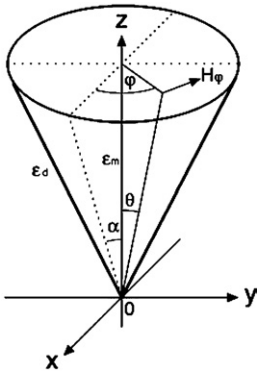

Figure 1. Geometry of a conical structure where superfocusing of SPPs occurs at a conical tip. Conical SPP modes are obtained by solving the wave equation of the magnetic field of the azimuthal component H_φ in the spherical coordinates system.

$$H_\varphi(r,\theta,t) = \mathrm{Re}[H_\varphi(r,\theta)\,\mathrm{e}^{-\mathrm{i}\omega t}]. \tag{2}$$

Here, ω is the angular frequency of interest and c is the velocity of light in the vacuum.

In the superfocusing phenomena, the magnetic field localizes within about a half wavelength's distance of the cone's surface. In spherical coordinates, this means that the θ distribution of $H_\varphi(r,\theta)$ becomes narrower with increasing radius r. In other words, the θ distribution of $H_\varphi(r,\theta)$ becomes broader as the cone's apex is approached. This mathematical behavior cannot be easily expressed by fundamental solutions based on the conventional separation of variables approach, in which the magnetic field is usually written as $H_\varphi(r,\theta) = R(r)\Psi(\theta)$ on the implicit assumption that the θ distribution is invariable against changes of r or depends on θ alone. To readily obtain solutions appropriate for the superfocusing phenomena, let us tentatively replace $\Psi(\theta)$ with $\Psi(\theta,r)$ and write the corresponding magnetic field as

$$H_\varphi(r,\theta) = R(r)\Psi(\theta,r), \tag{3}$$

where $\Psi(\theta,r)$ cannot be yet determined as a unique solution and is further assumed to be

$$\Psi(\alpha,r) = 1, \tag{4}$$

which is the boundary condition at the cone surface to express $\Psi(\theta,r)$ as the θ distribution of $H_\varphi(r,\theta)$. If our attempt succeeds, equations (3) and (4) will be justified. Substituting equation (3) into equation (1), we get

$$-\left(\frac{r}{R(r)}\frac{\partial^2}{\partial r^2}rR(r)+\varepsilon_j\frac{\omega^2}{c^2}r^2\right) = \left(\frac{1}{\Psi(\theta,r)}\frac{\partial}{\partial\theta}\frac{1}{\sin\theta}\frac{\partial}{\partial\theta}\Psi(\theta,r)\sin\theta+\frac{r^2}{\Psi(\theta,r)}\frac{\partial^2}{\partial r^2}\Psi(\theta,r)\right.$$
$$\left.+\frac{2r}{R(r)\Psi(\theta,r)}\left(\frac{\partial}{\partial r}rR(r)\right)\frac{\partial}{\partial r}\Psi(\theta,r)\right), \qquad j=m,d. \tag{5}$$

Equation (5) exhibits one exclusive separation of variables. The left side of equation (5) depends on r and the right side depends on r and θ. If equation (5) is to hold for arbitrary values of θ, each side must be equal to an invariant quantity with respect to θ or a function of r alone. We choose

$$\frac{r}{R(r)}\frac{\partial^2}{\partial r^2}rR(r)+\varepsilon_j\frac{\omega^2}{c^2}r^2 = -\zeta_j(r), \qquad j=m,d \tag{6}$$

$$\frac{1}{\Psi(\theta,r)}\frac{\partial}{\partial\theta}\frac{1}{\sin\theta}\frac{\partial}{\partial\theta}\Psi(\theta,r)\sin\theta+\frac{r^2}{\Psi(\theta,r)}\frac{\partial^2}{\partial r^2}\Psi(\theta,r)$$
$$+\frac{2r}{R(r)\Psi(\theta,r)}\left(\frac{\partial}{\partial r}rR(r)\right)\frac{\partial}{\partial r}\Psi(\theta,r)=\zeta_j(r),\qquad j=m,d. \tag{7}$$

Multiplying equation (6) by $R(r)/r^2$ and rearranging terms, we have for the radial equation that

$$\frac{\partial^2}{\partial r^2}R(r)+\frac{2}{r}\frac{\partial}{\partial r}R(r)+\left(\frac{\zeta_j(r)}{r^2}+\varepsilon_j\frac{\omega^2}{c^2}\right)R(r)=0,\qquad j=m,d. \tag{8}$$

Multiplying equation (7) by $\Psi(\theta,r)$ and rearranging terms, we have for the extended polar angle equation that

$$\frac{\partial}{\partial\theta}\frac{1}{\sin\theta}\frac{\partial}{\partial\theta}\Psi(\theta,r)\sin\theta-\zeta_j(r)\Psi(\theta,r)=-F(\theta,r),\qquad j=m,d \tag{9}$$

$$F(\theta,r)=r^2\frac{\partial^2}{\partial r^2}\Psi(\theta,r)+\frac{2r}{R(r)}\left(\frac{\partial}{\partial r}rR(r)\right)\frac{\partial}{\partial r}\Psi(\theta,r). \tag{10}$$

The above method is a simple extension of the separation of variables approach, and can thus be referred to as a quasi-separation of variables. Each quasi-separation introduces an arbitrary invariant of quasi-separation in much the same way as each separation introduces an arbitrary constant of separation.

From the Maxwell equations in the Gaussian system, we can determine the electric field $\boldsymbol{E}(t)$ $(E_r(t), E_\theta(t), E_\varphi(t))$ related to the magnetic field. Setting

$$(E_r(t),E_\theta(t),E_\varphi(t))=\mathrm{Re}[(E_r,E_\theta,E_\varphi)\,\mathrm{e}^{-\mathrm{i}\omega t}], \tag{11}$$

we obtain

$$E_r=E_r(r,\theta)=\frac{\mathrm{i}c}{\omega\varepsilon_j}\frac{1}{r\sin\theta}\frac{\partial}{\partial\theta}(H_\varphi(r,\theta)\sin\theta),\qquad j=m,d \tag{12}$$

$$E_\theta=E_\theta(r,\theta)=-\frac{\mathrm{i}c}{\omega\varepsilon_j}\frac{1}{r}\frac{\partial}{\partial r}(rH_\varphi(r,\theta)),\qquad j=m,d \tag{13}$$

and

$$E_\varphi=0,\qquad j=m,d. \tag{14}$$

The boundary conditions of the electric field in the radial component on the interface at the polar angle $\theta=\alpha$ allow us to determine the value of $\zeta_j(r)$.

3. The radial equation for the magnetic field

We first consider the radial equation (8), a pair of ODEs with respect to r distinguished by metallic and dielectric regions, and discuss it in the two limiting cases of $r\to\infty$ and $r\to 0$ where SPPs in conical geometry are well understood. For $r\to\infty$, the SPPs in conical geometry approach the SPPs in plane geometry. For $r\to 0$, the SPPs in conical geometry were studied by Babadjanyan *et al* [12].

In the case of $r\to\infty$, the radial equation (8) becomes

$$\frac{\partial^2}{\partial r^2}R(r)+\frac{2}{r}\frac{\partial}{\partial r}R(r)+\left(\frac{\zeta_j(\infty)}{r^2}+\varepsilon_j\frac{\omega^2}{c^2}\right)R(r)=0,\qquad j=m,d. \tag{15}$$

When the conservation law of energy flow in the closed spherical space, or Sommerfeld's radiation condition [26], is taken into consideration, the elementary solutions to equation (15) should have the form

$$R(r) = \frac{\exp(\pm \mathrm{i} k_p r)}{r} \qquad \text{for} \quad r \to \infty \tag{16}$$

where k_p is a wave number of the SPPs in planar geometry given by [30]

$$k_p = \frac{\omega}{c}\sqrt{\frac{\varepsilon_m \varepsilon_d}{\varepsilon_m + \varepsilon_d}}. \tag{17}$$

In this case, $\Psi(\theta, r)$ is easily written in the form

$$\Psi(\theta, r) = \exp(-\beta_j r_\perp), \qquad j = m, d \qquad \text{for} \quad r \to \infty \tag{18}$$

with

$$r_\perp = r|\sin(\theta - \alpha)| \tag{19}$$

$$\beta_j = \sqrt{k_p^2 - \varepsilon_j \frac{\omega^2}{c^2}}, \qquad j = m, d \tag{20}$$

where $r_\perp$ is the distance from the cone surface $\theta = \alpha$ and β_j are the imaginary wave numbers of planar SPPs in medium j, perpendicular to the planar structure. Near the cone surface $\theta \approx \alpha$, equation (18) is approximately

$$\Psi(\theta, r) \approx \exp(-\beta_j r|\theta - \alpha|), \qquad j = m, d \qquad \text{for} \quad r \to \infty \quad \text{and} \quad |\theta - \alpha| \approx 0 \tag{21}$$

which is further discussed in appendix C. With the substitution of equation (16) into equation (15), the radial equation (15) becomes independent of medium j as follows:

$$\frac{\partial^2}{\partial r^2} R(r) + \frac{2}{r}\frac{\partial}{\partial r} R(r) + k_p^2 R(r) = 0 \qquad \text{for} \quad r \to \infty \tag{22}$$

and we find the relation

$$\frac{\zeta_j(\infty)}{r^2} = \beta_j^2, \qquad j = m, d \qquad \text{for} \quad r \to \infty. \tag{23}$$

For $r \to 0$, the radial equation (8) becomes

$$\frac{\partial^2}{\partial r^2} R(r) + \frac{2}{r}\frac{\partial}{\partial r} R(r) + \left(\frac{\zeta_j(0)}{r^2} + \varepsilon_j \frac{\omega^2}{c^2}\right) R(r) = 0, \qquad j = m, d \qquad \text{for} \quad r \to 0, \tag{24}$$

which can be further simplified according to Babadjanyan *et al* [12] into the form

$$\frac{\partial^2}{\partial r^2} R(r) + \frac{2}{r}\frac{\partial}{\partial r} R(r) + \frac{\zeta_j(0)}{r^2} R(r) = 0, \qquad j = m, d \qquad \text{for} \quad r \to 0 \tag{25}$$

if we assume that

$$\frac{|\zeta_j(0)|}{r^2} \gg |\varepsilon_j| \frac{\omega^2}{c^2}, \qquad j = m, d \qquad \text{for} \quad r \to 0, \tag{26}$$

which is usually acceptable unless $\zeta_j(0) = 0$. Without the term ε_j in medium j, equation (25) does not distinguish a pair of differential equations in medium j and therefore it reduces to

$$\frac{\partial^2}{\partial r^2} R(r) + \frac{2}{r}\frac{\partial}{\partial r} R(r) + \frac{\zeta(0)}{r^2} R(r) = 0 \qquad \text{for} \quad r \to 0 \tag{27}$$

where we set

$$\zeta(0) = \zeta_m(0) = \zeta_d(0). \tag{28}$$

Now we are ready to consider a generalized radial equation containing equations (22) and (27) as limited cases. The simplest candidate equation is

$$\frac{\partial^2}{\partial r^2}R(r)+\frac{2}{r}\frac{\partial}{\partial r}R(r)+\left(k_p^2+\frac{\zeta(0)}{r^2}\right)R(r)=0 \qquad \text{for} \quad 0<r<\infty, \tag{29}$$

which becomes equations (22) and (27) in the respective limits. Most generally, we have

$$\frac{\partial^2}{\partial r^2}R(r)+\frac{2}{r}\frac{\partial}{\partial r}R(r)+\left(k_p^2+\frac{\zeta(0)+A(r)}{r^2}\right)R(r)=0 \qquad \text{for} \quad 0<r<\infty \tag{30}$$

where $A(r)$ is arbitrary only if

$$\lim_{r\to 0}A(r)=0, \qquad \lim_{r\to\infty}A(r)/r^2=0. \tag{31}$$

By setting

$$A(r)=\zeta(r)-\zeta(0) \tag{32}$$

in equation (30), we can generally write

$$\frac{\partial^2}{\partial r^2}R(r)+\frac{2}{r}\frac{\partial}{\partial r}R(r)+\left(k_p^2+\frac{\zeta(r)}{r^2}\right)R(r)=0 \qquad \text{for} \quad 0<r<\infty \tag{33}$$

where $\zeta(r)$ is arbitrary only if

$$\lim_{r\to\infty}\zeta(r)/r^2=0. \tag{34}$$

Here, $\zeta(r)$ is a newly defined function, which is different from $\zeta_j(r)$, $j=m,\,d$. Comparing equations (8) and (33), we find the useful relation

$$\frac{\zeta_j(r)}{r^2}=\beta_j^2+\frac{\zeta(r)}{r^2}, \qquad j=m,d \qquad \text{for} \quad 0<r<\infty, \tag{35}$$

which includes equation (23). What is important here is that the pair of ODEs distinguished by metallic and dielectric regions in equation (8) can be unified into a single ODE independent of those regions in equation (33) if the pair satisfies condition (35). Hence, we call equation (35) the unification conditions. Moreover, the pair of quasi-separation invariants in $\zeta_j(r)$, $j=m,\,d$, is unified into the single function $\zeta(r)$, which is then called a unified quasi-separation invariant.

Further discussion on the unified radial equation (33) would require more detailed information on the unified quasi-separation invariant $\zeta(r)$, which can be determined from the boundary conditions.

4. Application of perturbation methods to the extended polar angle equation for the magnetic field

In the preceding section, the unified quasi-separation invariant $\zeta(r)$ is introduced for obtaining the unified radial equation (33). In this section, we also use $\zeta(r)$ for the extended polar angle equation (9). Writing equation (35) in the form

$$\zeta_j(r)=(\beta_j r)^2+\zeta(r) \tag{36}$$

and substituting equation (36) into the extended polar angle equation (9), we obtain

$$\frac{\partial}{\partial\theta}\frac{1}{\sin\theta}\frac{\partial}{\partial\theta}\Psi(\theta,r)\sin\theta-\{(\beta_j r)^2+\zeta(r)\}\Psi(\theta,r)=-F(\theta,r), \qquad j=m,d \tag{37}$$

with

$$F(\theta, r) = r^2 \frac{\partial^2}{\partial r^2}\Psi(\theta, r) + 2r\left(R(r) + \frac{r}{R(r)}\frac{\partial R(r)}{\partial r}\right)\frac{\partial}{\partial r}\Psi(\theta, r) \tag{38}$$

from equation (10).

We are now faced with the problem of solving the extended polar angular equation (37), which is a PDE with respect to θ and r including the radial function $R(r)$ not yet determined. The left side of equation (37) originates from the polar angle equation in ordinary separation of variables for the apex point, and it can be exactly solved as was done by Babadjanyan *et al* [12]. This suggests that perturbation methods [31] can be applied to equation (37) as a perturbing term $F(\theta, r)$ on the right side. According to perturbation theory, let us introduce the perturbation parameter $0 \leqslant \varepsilon \leqslant 1$ into equation (37) and consider the perturbed equation

$$\frac{\partial}{\partial\theta}\frac{1}{\sin\theta}\frac{\partial}{\partial\theta}\Psi(\theta, r)\sin\theta - \{(\beta_j r)^2 + \zeta(r)\}\Psi(\theta, r) = -\varepsilon F(\theta, r), \qquad j = m, d. \tag{39}$$

We look for a solution of the form

$$\Psi(\theta, r) = \Psi^{(0)}(\theta, r) + \varepsilon\Psi^{(1)}(\theta, r) + \varepsilon^2\Psi^{(2)}(\theta, r) + \cdots \tag{40}$$

which satisfies

$$\Psi(\alpha, r) = \Psi^{(0)}(\alpha, r) + \varepsilon\Psi^{(1)}(\alpha, r) + \varepsilon^2\Psi^{(2)}(\alpha, r) + \cdots = 1 \tag{41}$$

when equation (40) for $\theta = \alpha$ is set equal to one from equation (4). Accordingly, $\zeta(r)$ and $R(r)$ should be described as a power series in ε:

$$\zeta(r) = \zeta^{(0)}(r) + \varepsilon\zeta^{(1)}(r) + \varepsilon^2\zeta^{(2)}(r) + \cdots \tag{42}$$

$$R(r) = R^{(0)}(r) + \varepsilon R^{(1)}(r) + \varepsilon^2 R^{(2)}(r) + \cdots. \tag{43}$$

Substituting equations (40) and (42) into the perturbed equation (39) and setting the coefficients of the powers of ε equal to each other, we find for the zeroth-order equation that

$$\frac{\partial}{\partial\theta}\frac{1}{\sin\theta}\frac{\partial}{\partial\theta}\Psi^{(0)}(\theta, r)\sin\theta - \{(\beta_j r)^2 + \zeta^{(0)}(r)\}\Psi^{(0)}(\theta, r) = 0, \qquad j = m, d, \tag{44}$$

with the boundary condition

$$\Psi^{(0)}(\alpha, r) = 1 \tag{45}$$

from equation (41). In the same way, we have for the first-order equation that

$$\begin{aligned}\frac{\partial}{\partial\theta}\frac{1}{\sin\theta}\frac{\partial}{\partial\theta}\Psi^{(1)}(\theta, r)\sin\theta - \{(\beta_j r)^2 + \zeta^{(0)}(r)\}\Psi^{(1)}(\theta, r)\\ = -\left[r^2\frac{\partial^2}{\partial r^2}\Psi^{(0)}(\theta, r) + 2r\left(R^{(0)}(r) + \frac{r}{R^{(0)}(r)}\frac{\partial R^{(0)}(r)}{\partial r}\right)\frac{\partial}{\partial r}\Psi^{(0)}(\theta, r)\right.\\ \left. - \zeta^{(1)}(r)\Psi^{(0)}(\theta, r)\right], \qquad j = m, d,\end{aligned} \tag{46}$$

with the boundary condition

$$\Psi^{(1)}(\alpha, r) = 0. \tag{47}$$

Our considerations in this paper are limited to the zeroth-order equation (44) for the extended polar angle equation (37). The first-order or higher-order equations will be discussed elsewhere.

5. The zeroth-order extended polar angle equation for the magnetic field

The zeroth-order extended polar angle equation (44) is considered to be an ODE with respect to θ because r can be treated as a constant for the calculations. If $g(\theta, r)$ is a solution to ODE (44), the solution satisfying the boundary condition (45) can be written in the form

$$\Psi^{(0)}(\theta, r) = g(\theta, r)/g(\alpha, r). \tag{48}$$

Note that equation (48) also gives a closely approximate solution around the conical surface $\theta = \alpha$ to the original polar extended angle equation (9) because the perturbing term $F(\theta, r) \to 0$ as $\theta \to \alpha$ (see appendix B). Equation (44) can be transformed using $\cos\theta = x$ into the associated Legendre differential equation [32]

$$(1-x^2)\frac{\mathrm{d}^2}{\mathrm{d}x^2}\Psi^{(0)}(x,r) - 2x\frac{\mathrm{d}}{\mathrm{d}x}\Psi^{(0)}(x,r) + \left[l_j(r)\{l_j(r)+1\} - \frac{1}{1-x^2}\right]\Psi^{(0)}(x,r) = 0, \qquad j = m, d \tag{49}$$

where

$$l_j(r) = -\tfrac{1}{2} + \mathrm{i}\tau_j(r), \qquad \tau_j(r) = \sqrt{(\beta_j r)^2 + \zeta^{(0)}(r) - 1/4}. \tag{50}$$

Linearly independent solutions [32] to equation (49) are provided by associated Legendre functions of the first kind, $P^1_{-(1/2)+i\tau_j(r)}(x)$ and $P^1_{-(1/2)+i\tau_j(r)}(-x)$, which are called the conical functions [33]. Here, $P^1_{-(1/2)+i\tau_j(r)}(x)$ is a decreasing function defined in $-1 < x \leqslant 1$ with the values of 0 at $x = 1$ and $+\infty$ at $x = -1$. From equation (48), the solution satisfying the boundary condition (45) can be written in the form

$$\Psi^{(0)}(\theta, r) = \begin{cases} P^1_{-(1/2)+\mathrm{i}\tau_m(r)}(\cos\theta) \Big/ P^1_{-(1/2)+\mathrm{i}\tau_m(r)}(\cos\alpha), & \theta \leqslant \alpha \\ P^1_{-(1/2)+\mathrm{i}\tau_d(r)}(-\cos\theta) \Big/ P^1_{-(1/2)+\mathrm{i}\tau_d(r)}(-\cos\alpha), & \theta \geqslant \alpha \end{cases} \tag{51}$$

Note that, as $r \to \infty$ at $\theta \approx \alpha$, equation (51) approaches the extended angular function in planar geometry, equation (21), whose proof is given in appendix C.

Without detailed knowledge of the radial function, we can describe the boundary condition for the continuity of the radial electric field at the angle $\theta = \alpha$. In perturbation methods, the radial electric field is written as a power series in ε:

$$E_r(r) = E_r^{(0)}(r) + \varepsilon E_r^{(1)}(r) + \varepsilon^2 E_r^{(2)}(r) + \cdots. \tag{52}$$

Substituting equations (40), (43) and (52) into equation (12), and setting the coefficients of the powers of ε equal to each other, we find for the zeroth-order radial electric field that

$$E_r^{(0)}(r,\theta) = \frac{\mathrm{i}c}{\omega\varepsilon_j}\frac{1}{r\sin\theta}\frac{\partial}{\partial\theta}(R^{(0)}(r)\Psi^{(0)}(\theta, r)\sin\theta), \qquad j = m, d. \tag{53}$$

Substituting equation (51) into equation (53), we obtain

$$E_r^{(0)}(r,\theta) = \frac{\mathrm{i}c}{\omega}\frac{R^{(0)}(r)}{r}\begin{cases} \dfrac{1}{\varepsilon_m}\left[-\sin\theta\dfrac{P'^1_{-(1/2)+\mathrm{i}\tau_m(r)}(\cos\theta)}{P^1_{-(1/2)+\mathrm{i}\tau_m(r)}(\cos\alpha)} + \cot\theta\dfrac{P^1_{-(1/2)+\mathrm{i}\tau_m(r)}(\cos\theta)}{P^1_{-(1/2)+\mathrm{i}\tau_m(r)}(\cos\alpha)}\right], \\ \qquad \theta \leqslant \alpha \\ \dfrac{1}{\varepsilon_d}\left[\sin\theta\dfrac{P'^1_{-(1/2)+\mathrm{i}\tau_d(r)}(-\cos\theta)}{P^1_{-(1/2)+\mathrm{i}\tau_d(r)}(-\cos\alpha)} + \cot\theta\dfrac{P^1_{-(1/2)+\mathrm{i}\tau_d(r)}(-\cos\theta)}{P^1_{-(1/2)+\mathrm{i}\tau_d(r)}(-\cos\alpha)}\right], \\ \qquad \theta \geqslant \alpha \end{cases} \tag{54}$$

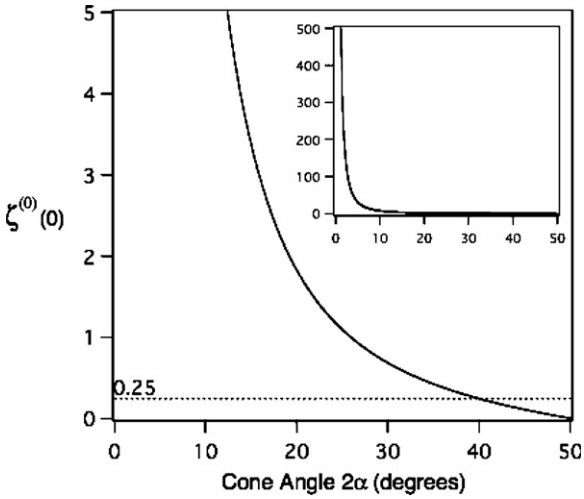

Figure 2. Numerical calculations of the zeroth-order unified quasi-separation invariant at $r = 0$, $\zeta^{(0)}(0)$, as a function of the cone angle 2α when $\varepsilon_d = 1$ and $\varepsilon_m = -20$ are used in equation (55). The broken line $\zeta^{(0)}(0) = 0.25$ shows the lower limit to $\nu > 0$, where the zeroth-order unified radial equation (64) is approximately solved by transforming it into the unmodified Bessel differential equation of purely imaginary order. The inset shows the original figure at a hundred times larger scale for the $\zeta^{(0)}(0)$-axis.

where $P'^{1}_{-(1/2)+\mathrm{i}\tau_j(r)}(x) = \partial_x P^{1}_{-(1/2)+\mathrm{i}\tau_j(r)}(x)$ for $j = m, d$. The continuity of the zeroth-order radial electric field at the polar angle $\theta = \alpha$ thus gives the form

$$\frac{1}{\varepsilon_m}\left[-\sin\alpha\frac{P'^{1}_{-(1/2)+\mathrm{i}\tau_m(r)}(\cos\alpha)}{P^{1}_{-(1/2)+\mathrm{i}\tau_m(r)}(\cos\alpha)}+\cot\alpha\right]=\frac{1}{\varepsilon_d}\left[\sin\alpha\frac{P'^{1}_{-(1/2)+\mathrm{i}\tau_d(r)}(-\cos\alpha)}{P^{1}_{-(1/2)+\mathrm{i}\tau_d(r)}(-\cos\alpha)}+\cot\alpha\right], \quad (55)$$

which is the boundary condition to numerically determine the zeroth-order unified quasi-separation invariant $\zeta^{(0)}(r)$. Note that the continuity of the angular electric displacement, $\varepsilon_j E_\theta(r, \theta)$ in medium j, at $\theta = \alpha$ is automatically satisfied using equation (13) and provides no further conditions.

6. Algebraically approximate determination of the zeroth-order unified quasi-separation invariant

The zeroth-order unified quasi-separation invariant $\zeta^{(0)}(r)$ can be numerically determined by solving the boundary condition (55) with specific values of dielectric functions in metallic and dielectric matter. Assuming that the dielectric matter is air, the metallic cone is gold and the light is at about 750 nm wavelength, we use $\varepsilon_d = 1$ for the dielectric matter and $\varepsilon_m = -20$ for the metallic cone in the numerical calculations. Although the experimental dielectric function of the metallic cone is $\varepsilon_m = -20.6 + 1.57\mathrm{i}$ at the 750 nm wavelength [34], the imaginary part is much smaller than the real part and is thus ignored for the sake of simplicity. Figure 2 shows $\zeta^{(0)}(0)$ as a function of the cone angle 2α. In figure 3, the solid lines show $\zeta^{(0)}(r) - \zeta^{(0)}(0)$ for specific cone angles as a function of r/λ_0, where λ_0 $(= 2\pi c/\omega)$ is the wavelength in vacuum. Figure 3 also shows the broken lines that are fitting curves for the solid lines in the range of $0 \leqslant r/\lambda_0 \leqslant 2$ and are consequently unclear due to their overlapping with the solid lines. If the fitting range is broader, the differences between broken and solid lines are clearly observed.

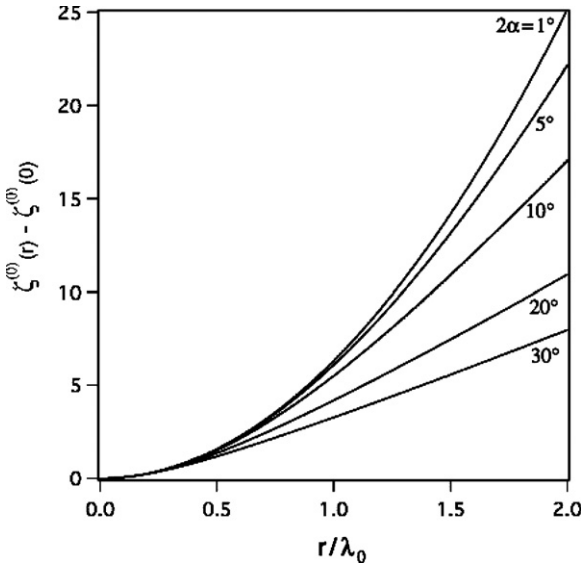

Figure 3. Numerical calculations of the zeroth-order unified quasi-separation invariant $\zeta^{(0)}(r)$ as a function of the radius r for various cone angles 2α when $\varepsilon_d = 1$ and $\varepsilon_m = -20$ are used in equation (55). For convenience of explanation, $\zeta^{(0)}(r) - \zeta^{(0)}(0)$ is shown. Broken lines are fitting curves that are not clear because of their overlapping with the solid lines obtained from the numerical calculations.

Here we here use a fitting function with two parameters, p and q, in the form

$$\begin{aligned}\zeta^{(0)}(r) - \zeta^{(0)}(0) &= (p\lambda_0)\left[(r/\lambda_0) + (q/\lambda_0)\left\{\exp\left(-\frac{(r/\lambda_0)}{(q/\lambda_0)}\right) - 1\right\}\right] \\ &= p[r + q\{\exp(-r/q) - 1\}] \end{aligned} \tag{56}$$

which is the same as the equation obtained for free fall motion with air resistance proportional to the velocity. The fitting function (56) is well known by physicists to be a function of r that shows a square increase around $r = 0$ and a linear increase at large r. Its behavior is approximate for $\zeta^{(0)}(r)$ in equation (55) (see appendix D). In $r \ll q$, equation (56) approximates a square function of r as follows:

$$\zeta^{(0)}(r) - \zeta^{(0)}(0) = p\left\{\frac{r^2}{2!q} - \frac{r^3}{3!q^2} + \cdots + (-1)^n\frac{r^n}{n!q^{n-1}} + \cdots\right\} \approx \frac{p}{2q}r^2 \qquad \text{for} \quad r \ll q. \tag{57}$$

Table 1 shows several values of p and q normalized to the wavelength in vacuum, λ_0. The values of q/λ_0 indicate the effective range of r/λ_0 in the approximation (57). The values of $p/2q$ normalized to the wavelength, λ_0, are used in the following sections. For convenience, equation (57) is rewritten in the form

$$\zeta^{(0)}(r) \approx \zeta^{(0)}(0) + ar^2 \qquad \text{for} \quad r \ll q \tag{58}$$

where

$$a = \frac{p}{2q}. \tag{59}$$

Table 1. Values of the parameters in equations (56)–(59) used for solving equation (65). Fitting parameters of p and q in equation (56) were obtained by fitting the curves in figure 3. Fitting parameters are normalized by the wavelength in vacuum, λ_0. The values of $p\lambda_0^2/2q$ conveniently replaced by $a\lambda_0^2$ appear in the approximation of the zeroth-order unified quasi-separation invariant $\zeta^{(0)}(r)$ in equation (58). The values of $\zeta^{(0)}(0)$ are obtained from the boundary condition in equation (55) when $r = 0$.

2α (degrees)	$p\lambda_0$	q/λ_0	$p\lambda_0^2/2q\ (= a\lambda_0^2)$	$\zeta^{(0)}(0)$
1	349.9	27.24	6.422	798.3
5	43.69	3.233	6.756	31.80
10	15.27	1.027	7.433	7.839
20	7.053	0.4586	7.689	1.834
30	4.713	0.3170	7.434	0.6888

Table 2. Values of the parameters in equations (56)–(59) numerically calculated from equations (60)–(63) for comparison with table 1. There is a great difference in the corresponding data values between tables 1 and 2.

2α (degrees)	$p\lambda_0$	q/λ_0	$p\lambda_0^2/2q\ (= a\lambda_0^2)$	$\zeta^{(0)}(0)$
1	8.326	0.100 2	41.56	16 040
5	1.665	0.020 04	41.56	641.9
10	0.8326	0.010 02	41.56	160.7
20	0.4163	0.005 009	41.56	40.35
30	0.2775	0.003 339	41.56	18.07

In appendix D, we obtain such approximate expressions as

$$p \approx \frac{2}{\alpha}\left(\frac{\varepsilon_m - \varepsilon_d}{\varepsilon_m\beta_m - \varepsilon_d\beta_d}\right) \tag{60}$$

$$q \approx \frac{1}{\alpha k_p^2}\left(\frac{\varepsilon_m - \varepsilon_d}{\varepsilon_m\beta_m - \varepsilon_d\beta_d}\right) \tag{61}$$

$$a \approx k_p^2 \tag{62}$$

$$\zeta^{(0)}(0) \approx \frac{1}{\alpha^2}\left(\frac{\varepsilon_m - \varepsilon_d}{\varepsilon_m + \varepsilon_d}\right)^2 + \frac{1}{4}, \tag{63}$$

which are used in forming table 2. Unfortunately, there is a great difference in the corresponding numerical values between tables 1 and 2. Consequently, equations (60)–(63) are too roughly approximated to use them for the asymptotic expression of $\zeta^{(0)}(r)$ in the following section. We have no choice but to use the fitting parameters in table 1 until a suitable asymptotic expression for $\zeta^{(0)}(r)$ is found.

7. Analytically approximate solutions to the zeroth-order unified radial equation for the magnetic field

Substituting equations (42) and (43) into the unified radial equation (33), and setting the coefficients of the powers of ε equal to each other, we find for the zeroth-order unified radial equation that

$$\frac{\partial^2}{\partial r^2}R^{(0)}(r) + \frac{2}{r}\frac{\partial}{\partial r}R^{(0)}(r) + \left(k_p^2 + \frac{\zeta^{(0)}(r)}{r^2}\right)R^{(0)}(r) = 0 \qquad \text{for} \quad 0 < r < \infty. \tag{64}$$

In the preceding section, the zeroth-order unified quasi-separation invariant $\zeta^{(0)}(r)$ was numerically determined and expressed as an appropriate fitting function in equation (56). Here, we consider a simple case where the differential equation (64) can be easily solved. For the approximate equation (58), equation (64) becomes

$$\frac{\partial^2}{\partial r^2}R^{(0)}(r)+\frac{2}{r}\frac{\partial}{\partial r}R^{(0)}(r)+\left(k_p^2+a+\frac{\zeta^{(0)}(0)}{r^2}\right)R^{(0)}(r)=0, \tag{65}$$

which is transformed using $R^{(0)}(r)=w(z)/\sqrt{z}$, $z=k_{mp}r$ and $k_{mp}=\sqrt{k_p^2+a}$ into the unmodified Bessel differential equation of purely imaginary order as follows:

$$\frac{\partial^2 w(z)}{\partial z^2}+\frac{1}{z}\frac{\partial w(z)}{\partial z}+\left(1-\frac{(\mathrm{i}\nu)^2}{z^2}\right)w(z)=0 \tag{66}$$

where

$$\nu=\sqrt{\zeta^{(0)}(0)-1/4}. \tag{67}$$

Here, to simplify the explanation, we consider only the case of $\nu>0$, which corresponds to $2\alpha<\sim 39.9^\circ$ in figure 2. As a pair of independent solutions of Bessel equation (66), we choose the Hankel functions $H_{\mathrm{i}\nu}^{(1)}(z)$ and $H_{\mathrm{i}\nu}^{(2)}(z)$ that correspond to the outgoing wave away from the conical tip and the incoming wave that propagates toward it, respectively, as the asymptotic behavior [35] as $z\to\infty$. In the superfocusing mode, our attention is focused on the incident wave expressed by the incoming wave $H_{\mathrm{i}\nu}^{(2)}(z)$. The reflected wave expressed by the outgoing wave $H_{\mathrm{i}\nu}^{(1)}(z)$ is a secondary matter for small cone angles (see equation (A.25) in appendix A). Thus, let us write a solution to equation (65) for the superfocusing mode as

$$R^{(0)}(r)=H_{\mathrm{i}\nu}^{(2)}(k_{mp}r)\big/\sqrt{k_{mp}r}. \tag{68}$$

According to (5.14) with (5.3), (5.9) and (5.10) in [35] and with (7.11) of chapter 10 in [36], the asymptotic expansion for $H_{\mathrm{i}\nu}^{(2)}(\nu z)$ is given by

$$H_{\mathrm{i}\nu}^{(2)}(\nu z)=\mathrm{e}^{-\nu\pi/2}\left(\frac{2}{\pi\nu}\right)^{1/2}(1+z^2)^{-1/4}\exp[-\mathrm{i}(\nu\xi(z)-\pi/4)]\left(1-\frac{U_1(u(z))}{\mathrm{i}\nu}+\cdots\right) \tag{69}$$

where

$$\xi(z)=(1+z^2)^{1/2}+\ln\left(\frac{z}{1+(1+z^2)^{1/2}}\right) \tag{70}$$

$$U_1(u(z))=\frac{3u(z)-5\{u(z)\}^3}{24} \tag{71}$$

$$u(z)=(1+z^2)^{-1/2}. \tag{72}$$

From equations (71) and (72), we obtain $|U_1(u(z))|\leqslant 2/\sqrt{5}\,(\approx 0.8944)$. When $\nu\gg\max|U_1(u(z))|=2/\sqrt{5}$, $H_{\mathrm{i}\nu}^{(2)}(\nu z)$ in equation (69) can be approximated to the form

$$H_{\mathrm{i}\nu}^{(2)}(\nu z)\approx\mathrm{e}^{-\nu\pi/2}\left(\frac{2}{\pi\nu}\right)^{1/2}(1+z^2)^{-1/4}\exp[-\mathrm{i}(\nu\xi(z)-\pi/4)]\qquad\text{for}\quad\nu\gg 2/\sqrt{5}. \tag{73}$$

In the substitution $z=k_{mp}r/\nu$ into equation (73), the zeroth-order radial function, $R^{(0)}(r)$, in equation (68) is approximated as

$$R^{(0)}(r)\approx\mathrm{e}^{-\nu\pi/2}\sqrt{\frac{2}{\pi\mu(r)k_{mp}r}}\exp\left[-\mathrm{i}\left(\mu(r)+\nu\ln\left(\frac{k_{mp}r}{\nu+\mu(r)}\right)-\pi/4\right)\right]$$
$$\text{for}\quad\nu\gg 2/\sqrt{5} \tag{74}$$

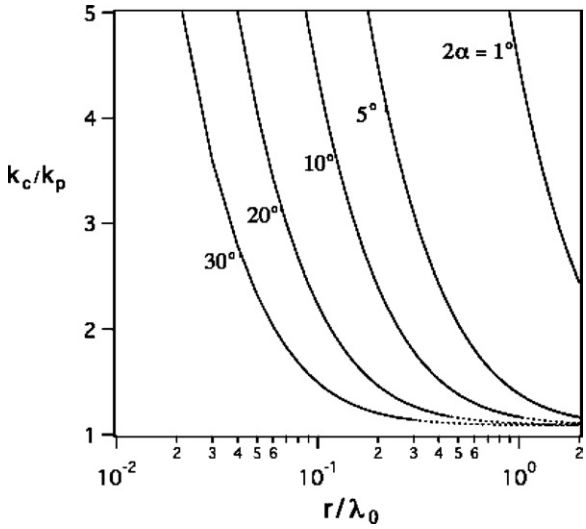

Figure 4. Numerical calculations of the wave number of conical SPPs normalized by that of planar SPPs, $k_c(r)/k_p$, as a function of the radius r for specific cone angles 2α when $\varepsilon_d = 1$ and $\varepsilon_m = -20$ are used in equation (76). The broken line does not satisfy the condition of the approximation denoted by $r < q$ in equation (57). Specific values of q for various cone angles 2α are shown in table 1.

where

$$\mu(r) = \sqrt{k_{mp}^2 r^2 + \nu^2}. \tag{75}$$

Differentiating the phase in equation (74) with respect to radius r, we obtain the wave number of the conical surface plasmons, $k_c(r)$, in the zeroth-order perturbation as follows:

$$k_c(r) = \frac{\mathrm{d}}{\mathrm{d}r}\left[\mu(r) + \nu \ln\left(\frac{k_{mp} r}{\nu + \mu(r)}\right) - \pi/4\right] = \frac{\nu}{r} + \frac{k_{mp}^2 r}{\nu + \mu(r)}, \tag{76}$$

which is more accurate than the previously used form [1, 12]

$$k_c(r) \approx \nu/r. \tag{77}$$

Either of equations (76) and (77) means that the wave number of the conical SPPs anomalously increases closer to the apex of the cone. Equation (76) is, however, more appropriate for describing the gradual transition from propagating to localized SPPs; this is shown by numerical calculations of $k_c(r)/k_p$ using equation (76) for the specific cone angles as a function of r/λ_0 (figure 4).

8. Electric field-line patterns of superfocusing modes in the zeroth-order perturbation

Field-line patterns are more sophisticated graphical representations of electromagnetic fields than field-vector patterns because of their simpler description. When the electromagnetic field has only an azimuthal component of the magnetic field that depends only on radius r and polar angle θ in spherical coordinates, we can obtain a time-varying scalar field whose contours represent the field-line pattern for the electric field that is derived from the magnetic field.

The tangent at an arbitrary point of an electric field line indicates the direction of the electric field vector $\boldsymbol{E}(r,\theta,t)$ at this point. This fact can be described mathematically by using a line vector element $\mathrm{d}\boldsymbol{s}$ as follows:

$$\boldsymbol{E}(r,\theta,t)\times d\boldsymbol{s}=0 \tag{78}$$

which can be simplified into the form

$$\frac{\mathrm{d}r}{E_r(r,\theta,t)}-\frac{r\,\mathrm{d}\theta}{E_\theta(r,\theta,t)}=0 \tag{79}$$

when

$$\boldsymbol{E}(r,\theta,t)=E_r(r,\theta,t)\,\boldsymbol{e}_r+E_\theta(r,\theta,t)\,\boldsymbol{e}_\theta \tag{80}$$

$$\mathrm{d}\boldsymbol{s}=\mathrm{d}r\,\boldsymbol{e}_r+r\,\mathrm{d}\theta\,\boldsymbol{e}_\theta \tag{81}$$

where $\boldsymbol{e}_r$ and $\boldsymbol{e}_\theta$ are the unit vectors to the r- and θ-axes, respectively. From equations (11) to (13) and equation (2), we obtain the r- and θ-components of the electric field as follows:

$$E_r(r,\theta,t)=\mathrm{Re}[E_r(r,\theta)\exp(-\mathrm{i}\omega t)]=\frac{c}{\omega\varepsilon_j}\frac{1}{r\sin\theta}\frac{\partial}{\partial\theta}\{H_\varphi(r,\theta,t')\sin\theta\} \tag{82}$$

$$E_\theta(r,\theta,t)=\mathrm{Re}[E_\theta(r,\theta)\exp(-\mathrm{i}\omega t)]=-\frac{c}{\omega\varepsilon_j}\frac{1}{r}\frac{\partial}{\partial r}\{rH_\varphi(r,\theta,t')\} \tag{83}$$

where

$$t'=t-\frac{\pi}{2\omega}. \tag{84}$$

Substituting equations (82) and (83) into equation (79), we obtain a differential equation expressed in terms of total derivatives with respect to r and θ as follows:

$$\sin\theta\frac{\partial}{\partial r}(rH_\varphi(r,\theta,t'))\,\mathrm{d}r+r\frac{\partial}{\partial\theta}(H_\varphi(r,\theta,t')\sin\theta)\,\mathrm{d}\theta=0, \tag{85}$$

which can be described by the exact differential form

$$\mathrm{d}\psi(r,\theta)=\frac{\partial}{\partial r}\psi(r,\theta)\,\mathrm{d}r+\frac{\partial}{\partial\theta}\psi(r,\theta)\,\mathrm{d}\theta=0 \tag{86}$$

with

$$\psi(r,\theta)=H_\varphi(r,\theta,t')r\sin\theta. \tag{87}$$

The solution is $\psi(r,\theta)=\mathrm{const}$, in which the time-varying scalar field for the electric field-line representation, denoted by $f(r,\theta,t)$, is proportional to the harmonic oscillation. This gives

$$f(r,\theta,t)=\mathrm{Re}[\mathrm{R}(r)\exp(-\mathrm{i}\omega t+\mathrm{i}\pi/2)]\Psi(\theta,r)r\sin\theta. \tag{88}$$

The field-line patterns at time $t=t_0$ are described by the scalar field with the contour

$$f(r,\theta,t_0)=C \tag{89}$$

where C is the contour level. The contour interval can be controlled by the interval value of the contour levels. The evolution of field-line patterns can be investigated for different moments

$$t=t_0+n\tau\qquad\text{with}\qquad n=0,1,2,3,\ldots \tag{90}$$

where τ is a suitable chosen duration between two neighboring snapshots. In perturbation methods, the time-varying scalar field for the electric field-line representation is written as a power series in ε:

$$f(r,\theta,t)=f^{(0)}(r,\theta,t)+\varepsilon f^{(1)}(r,\theta,t)+\varepsilon^2 f^{(2)}(r,\theta,t)+\cdots. \tag{91}$$

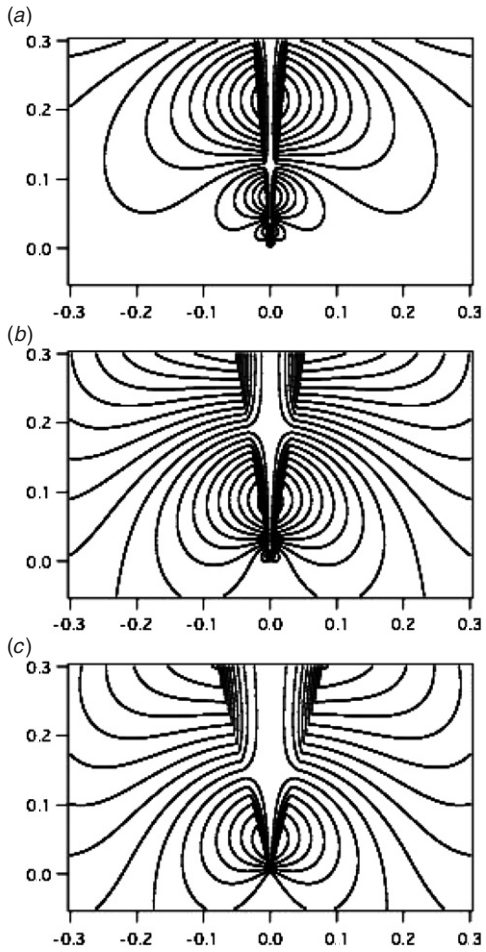

Figure 5. Electric field lines of the zeroth-order superfocusing mode of SPPs in conical geometry for the cone angle $2\alpha = 10^\circ$ (*a*), 20° (*b*) and 30° (*c*) at $t_0 = 0$. Geometrical dimensions of the horizontal and vertical axes are $r/\lambda_0 = 1$.

Substituting equations (40), (43) and (91) into equation (88), and setting the coefficients of the powers of ε equal to each other, we find for the zeroth-order perturbation that

$$f^{(0)}(r, \theta, t) = \mathrm{Re}[R^{(0)}(r) \exp(-\mathrm{i}\omega t + \mathrm{i}\pi/2)]\Psi^{(0)}(\theta, r) r \sin\theta. \tag{92}$$

In figure 5, electric field-line patterns of the zeroth-order superfocusing modes of conical SPPs for the cone angle $2\alpha = 10^\circ$ (a), 20° (b) and 30° (c) are described by equation (92) with the conditions of $\varepsilon_d = 1$, $\varepsilon_m = -20$ and $t_0 = 0$. In the calculations, we do not use the approximation to equation (74) in $R^{(0)}(r)$ when equation (68) is estimated. The geometrical dimensions in figure 5 are $r/\lambda_0 = 1$ on both the horizontal and vertical axes. Based on the values of q/λ_0 shown in table 1, all the areas in the three figures in figure 5 mostly satisfy the condition of equation (58), from which equation (68) is derived. The electric field-line patterns in figure 5 clearly show that the superfocusing phenomena occur more rapidly with increasing cone angle, which can be accounted for by the behavior of the wave number as a function of r in figure 4. In other words, with increasing cone angle, only a smaller area at the cone apex is allowed for localized SPPs whose wave number is much larger than that

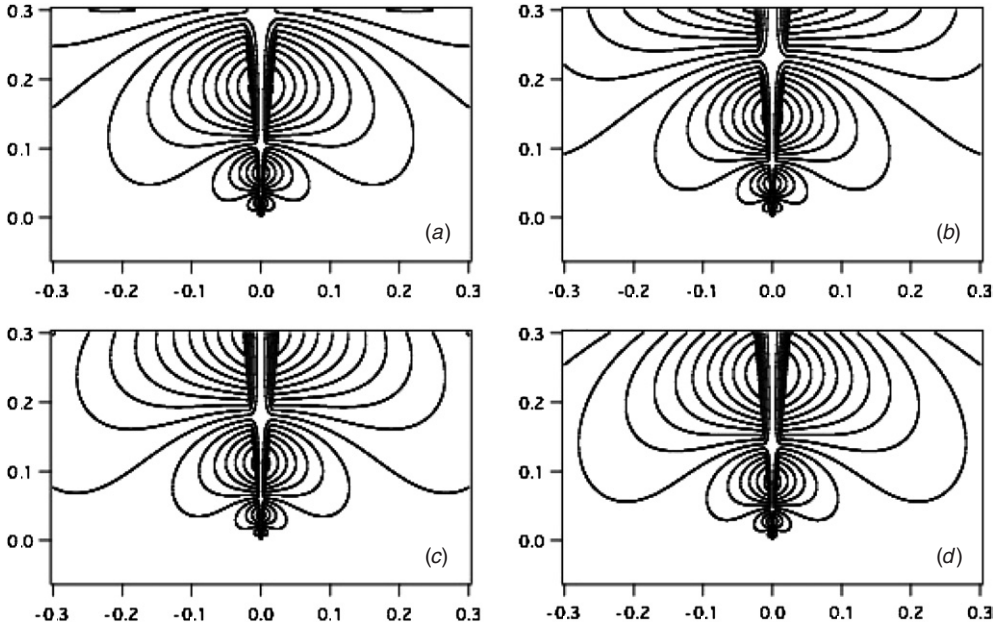

Figure 6. Pattern motion of electric field lines of the zeroth-order superfocusing mode of SPPs in conical geometry for cone angle $2\alpha = 10^\circ$ at different moments $t = t_0 + n\tau$ ($t_0 = T/16$, $\tau = T/8$ and $n = 0$ (*a*), 1 (*b*), 2 (*c*) and 3 (*d*)). Geometrical dimensions of the horizontal and vertical axes are $r/\lambda_0 = 1$.

of propagating SPPs. On the nanometer scale, the electric field would be extraordinarily enhanced for tapered nanoscale metal tips with smaller cone angles because a larger area at the cone apex is involved in localized SPPs.

In figure 6, the field-pattern evolution for the zeroth-order superfocusing mode of conical SPPs at cone angle $2\alpha = 10^\circ$ is represented for different moments $t = t_0 + n\tau$ for $n = 0$ (a), 1 (b), 2 (c) and 3 (d) with $t_0 = T/16$ and $\tau = T/8$, where T represents the time period ($T = 2\pi/\omega$). The field-pattern evolution is shown during a half-period $T/2$. $\varepsilon_d = 1$ and $\varepsilon_m = -20$ were used in the calculations, just as in figure 5. The geometrical dimensions are also $r/\lambda_0 = 1$ on both the horizontal and vertical axes. Figure 6 clearly shows that the field-pattern evolution shows a smaller change during half the time period in closer proximity to the cone apex because the group velocity of conical SPPs, $\omega/k_c(r)$, becomes slower. The computer-aided animation of the field-pattern evolution can give an intuitive understanding of the accumulation of superfocusing SPPs.

9. Concluding remarks and perspectives

We proposed a new analytic method based on the quasi-separation of variables for solving partial differential equations directly derived from the Maxwell equations and applied it to superfocusing problems for SPPs especially in conical geometry. The quasi-separation of variables combined with perturbation methods allows us to obtain an easily solvable set of homogeneous ordinary differential equations in the zeroth-order perturbation method. In the zeroth-order solution to superfocusing SPPs in conical geometry, we discussed cones with cone angles greater than previously considered and examined the wave number of conical

SPPs around the apex more carefully than has been done before. Electric field-line patterns around the apex of cones were expressed more exactly than is possible with the previously reported methods. In the new analytic method, more accurate considerations are possible because of the first-order or higher-order perturbation methods, in which a solvable set of nonhomogeneous ordinary differential equations is obtained (this will be discussed in detail elsewhere). We believe that this new analytic method is a powerful and useful technique for theoretically understanding superfocusing SPPs in other geometries such as wedge-shaped [15] and half two-sheet hyperboloidal geometries.

Acknowledgments

The authors are much indebted to Professors M Fukui and M Haraguchi of the University of Tokushima for their useful criticism on the quasi-separation of variables approach. The authors are also thankful to the reviewers for their comments that helped improve the quality of this paper.

Appendix A. Comments on the separation of variables approach taken by Babadjanyan *et al*

The ordinary separation of variables approach taken by Babadjanya *et al* [12] begins by assuming the magnetic field as

$$H_\varphi(r,\theta) = \bar{R}(r)\bar{\Psi}(\theta). \tag{A.1}$$

Substituting equation (A.1) into the wave equation (1), we get

$$\left(\frac{r}{\bar{R}(r)}\frac{\partial^2}{\partial r^2}r\bar{R}(r) + \varepsilon_j\frac{\omega^2}{c^2}r^2\right) + \frac{1}{\bar{\Psi}(\theta)}\frac{\partial}{\partial\theta}\frac{1}{\sin\theta}\frac{\partial}{\partial\theta}\bar{\Psi}(\theta)\sin\theta = 0, \qquad j = m, d. \tag{A.2}$$

Since the two terms are separately functions of r and θ respectively, each one must be constant:

$$\frac{r}{\bar{R}(r)}\frac{\partial^2}{\partial r^2}r\bar{R}(r) + \varepsilon_j\frac{\omega^2}{c^2}r^2 = -\bar{\zeta}_j, \qquad j = m, d \tag{A.3}$$

$$\frac{1}{\bar{\Psi}(\theta)}\frac{\partial}{\partial\theta}\frac{1}{\sin\theta}\frac{\partial}{\partial\theta}\bar{\Psi}(\theta)\sin\theta = \bar{\zeta}_j, \qquad j = m, d. \tag{A.4}$$

Here, $\bar{\zeta}_j$ for $j = m, d$ is the separation constant to be determined from the boundary conditions.

Multiplying equation (A.3) by $\bar{R}(r)$ and rearranging terms, we have for the radial equation that

$$\frac{\partial^2}{\partial r^2}\bar{R}(r) + \frac{2}{r}\frac{\partial}{\partial r}\bar{R}(r) + \left(\frac{\bar{\zeta}_j}{r^2} + \varepsilon_j\frac{\omega^2}{c^2}\right)\bar{R}(r) = 0, \qquad j = m, d. \tag{A.5}$$

For $r \to 0$, when the condition

$$\frac{|\bar{\zeta}_j|}{r^2} \gg |\varepsilon_j|\frac{\omega^2}{c^2}, \qquad j = m, d \tag{A.6}$$

is normally satisfied, the radial equation (A.5) becomes

$$\frac{\partial^2}{\partial r^2}\bar{R}(r) + \frac{2}{r}\frac{\partial}{\partial r}\bar{R}(r) + \frac{\bar{\zeta}_j}{r^2}\bar{R}(r) = 0, \qquad j = m, d \qquad \text{for} \quad r \to 0. \tag{A.7}$$

Without the term ε_j in medium j, equation (A.7) does not distinguish a pair of differential equations in medium j and therefore it reduces to

$$\frac{\partial^2}{\partial r^2}\bar{R}(r) + \frac{2}{r}\frac{\partial}{\partial r}\bar{R}(r) + \frac{\bar{\zeta}}{r^2}\bar{R}(r) = 0 \qquad \text{for} \quad r \to 0 \tag{A.8}$$

where we set

$$\bar{\zeta} = \bar{\zeta}_m = \bar{\zeta}_d. \tag{A.9}$$

Equation (A.8) is the final radial equation for describing the superfocusing phenomena based on the ordinary separation of variables approach. Comparing equation (A.8) with equation (65) described simply as

$$\frac{\partial^2}{\partial r^2} R^{(0)}(r) + \frac{2}{r}\frac{\partial}{\partial r} R^{(0)}(r) + \left(k_{mp}^2 + \frac{\zeta^{(0)}(0)}{r^2}\right) R^{(0)}(r) = 0, \tag{A.10}$$

we find the corresponding relationships between the ordinary and quasi-separations of variables approach as follows:

$$\bar{R}(r) = \lim_{k_{mp}\to 0} R^{(0)}(r) \tag{A.11}$$

$$\bar{\zeta} = \zeta^{(0)}(0). \tag{A.12}$$

The general solution of equation (A.8) for $r > 0$ is

$$\bar{R}(r) = a\frac{\exp[\mathrm{i}\nu \ln r]}{\sqrt{r}} + b\frac{\exp[-\mathrm{i}\nu \ln r]}{\sqrt{r}} \tag{A.13}$$

$$\nu = \sqrt{\bar{\zeta} - 1/4}, \tag{A.14}$$

where a and b are arbitrary constants. In contrast, the general solution of equation (A.10) for $r > 0$ is

$$R^{(0)}(r) = c\frac{F_{\mathrm{i}\nu}(k_{mp}r)}{\sqrt{k_{mp}r}} + d\frac{G_{\mathrm{i}\nu}(k_{mp}r)}{\sqrt{k_{mp}r}} \tag{A.15}$$

where $F_{\mathrm{i}\nu}(x)$ and $G_{\mathrm{i}\nu}(x)$ are two real independent solutions for unmodified Bessel functions of purely imaginary order, defined by Dunster [35] as

$$F_{\mathrm{i}\nu}(x) = \tfrac{1}{2}\left\{\mathrm{e}^{-\nu\pi/2} H_{\mathrm{i}\nu}^{(1)}(x) + \mathrm{e}^{\nu\pi/2} H_{\mathrm{i}\nu}^{(2)}(x)\right\} \tag{A.16}$$

$$G_{\mathrm{i}\nu}(x) = \tfrac{1}{2\mathrm{i}}\left\{\mathrm{e}^{-\nu\pi/2} H_{\mathrm{i}\nu}^{(1)}(x) - \mathrm{e}^{\nu\pi/2} H_{\mathrm{i}\nu}^{(2)}(x)\right\}. \tag{A.17}$$

Their behavior for small values of x is respectively described as

$$F_{\mathrm{i}\nu}(x) = \left(\frac{2\tanh(\nu\pi/2)}{\nu\pi}\right)^{1/2} \{\cos(\nu \ln(x/2) - \phi_{\nu,0}) + O(x^2)\}, \qquad x \to 0+ \tag{A.18}$$

$$G_{\mathrm{i}\nu}(x) = \left(\frac{2\coth(\nu\pi/2)}{\nu\pi}\right)^{1/2} \{\sin(\nu \ln(x/2) - \phi_{\nu,0}) + O(x^2)\}, \qquad x \to 0+ \tag{A.19}$$

where

$$\phi_{\nu,0} = \arg\{\Gamma(1 + \mathrm{i}\nu)\}. \tag{A.20}$$

As a superfocusing solution for the time dependence $\mathrm{e}^{-\mathrm{i}\omega t}$ in equation (2), we must set $a = 0$ in equation (A.13), obtaining

$$\bar{R}(r) = b\frac{\exp[-\mathrm{i}\nu \ln r]}{\sqrt{r}}, \tag{A.21}$$

which can be used to more accurately determine the zeroth-order radial function $R^{(0)}(r)$ according to the corresponding relationship in equation (A.11). Substituting equations (A.18) and (A.19) into equation (A.15), we obtain the general solution for small values of $k_{mp}r$ as follows:

$$R^{(0)}(r) = \frac{c}{\sqrt{k_{mp}r}}\left(\frac{2\tanh(\nu\pi/2)}{\nu\pi}\right)^{1/2}\{\cos(\nu\ln(k_{mp}r/2)-\phi_{\nu,0})\} + \frac{d}{\sqrt{k_{mp}r}}\left(\frac{2\coth(\nu\pi/2)}{\nu\pi}\right)^{1/2}\{\sin(\nu\ln(k_{mp}r/2)-\phi_{\nu,0})\}, \qquad k_{mp}r \to 0. \tag{A.22}$$

Comparing equations (A.21) and (A.22) with condition (A.11), we find that

$$c = b\sqrt{k_{mp}}\exp\left[\mathrm{i}\nu\ln\frac{k_{mp}}{2} - \mathrm{i}\phi_{\nu,0}\right]\left(\frac{2\tanh(\nu\pi/2)}{\nu\pi}\right)^{-1/2} \tag{A.23}$$

$$d = -\mathrm{i}b\sqrt{k_{mp}}\exp\left[\mathrm{i}\nu\ln\frac{k_{mp}}{2} - \mathrm{i}\phi_{\nu,0}\right]\left(\frac{2\coth(\nu\pi/2)}{\nu\pi}\right)^{-1/2}. \tag{A.24}$$

Substituting equations (A.23) and (A.24) into equation (A.15) and using equations (A.16) and (A.17) to express $R^{(0)}(r)$ in terms of Hankel functions, we obtain

$$R^{(0)}(r) = b\exp\left[\mathrm{i}\nu\ln\frac{k_{mp}}{2} - \mathrm{i}\phi_{\nu,0}\right]\left(\frac{2}{\nu\pi}\right)^{-1/2} \times\left(\frac{\sqrt{\coth(\nu\pi/2)}-\sqrt{\tanh(\nu\pi/2)}}{2}\,\mathrm{e}^{-\nu\pi/2}\,\frac{H_{\mathrm{i}\nu}^{(1)}(k_{mp}r)}{\sqrt{r}} + \frac{\sqrt{\coth(\nu\pi/2)}+\sqrt{\tanh(\nu\pi/2)}}{2}\,\mathrm{e}^{\nu\pi/2}\,\frac{H_{\mathrm{i}\nu}^{(2)}(k_{mp}r)}{\sqrt{r}}\right), \tag{A.25}$$

which is exact for the superfocusing solution of the zeroth-order radial function and more accurate than equation (68) in including the reflected outgoing wave described by the Hankel function of the first kind. If ν (equal to $\sqrt{\zeta^{(0)}-1/4}$) is large enough (physically corresponding to small cone angles in figure 2) to make the approximation

$$\tanh(\nu\pi/2) \approx 1 \tag{A.26}$$

$$\coth(\nu\pi/2) \approx 1, \tag{A.27}$$

equation (A.25) can be approximately expressed as

$$R^{(0)}(r) \approx b\exp\left[\mathrm{i}\nu\ln\frac{k_{mp}}{2} - \mathrm{i}\phi_{\nu,0}\right]\left(\frac{2}{\nu\pi}\right)^{-1/2}\mathrm{e}^{\nu\pi/2}\,\frac{H_{\mathrm{i}\nu}^{(2)}(k_{mp}r)}{\sqrt{r}}, \tag{A.28}$$

which is physically equivalent to the solution $R^{(0)}(r)$ in equation (68).

On the other hand, multiplying equation (A.4) by $\bar{\Psi}(\theta)$ and rearranging terms, we have for the polar angle equation that

$$\frac{\partial}{\partial\theta}\frac{1}{\sin\theta}\frac{\partial}{\partial\theta}\bar{\Psi}(\theta)\sin\theta - \bar{\zeta}_j\bar{\Psi}(\theta) = 0, \qquad j = m, d. \tag{A.29}$$

Comparing equation (A.29) with equation (44) described as

$$\frac{\partial}{\partial\theta}\frac{1}{\sin\theta}\frac{\partial}{\partial\theta}\Psi^{(0)}(\theta,r)\sin\theta - \{(\beta_j r)^2 + \zeta^{(0)}(r)\}\Psi^{(0)}(\theta,r) = 0, \qquad j = m, d, \tag{A.30}$$

we find the corresponding relationships as follows:

$$\bar{\Psi}(\theta) = \lim_{r\to 0} \Psi^{(0)}(\theta, r) \tag{A.31}$$

$$\bar{\zeta} = \zeta^{(0)}(0), \tag{A.32}$$

where equation (A.32) is the same as equation (A.12). Substituting equation (51) into equation (A.31), we obtain

$$\bar{\Psi}(\theta) = \begin{cases} P^1_{-(1/2)+\mathrm{i}\nu}(\cos\theta) \big/ P^1_{-(1/2)+\mathrm{i}\nu}(\cos\alpha), & \theta \leqslant \alpha \\ P^1_{-(1/2)+\mathrm{i}\nu}(-\cos\theta) \big/ P^1_{-(1/2)+\mathrm{i}\nu}(-\cos\alpha), & \theta \geqslant \alpha, \end{cases} \tag{A.33}$$

where $\nu = \sqrt{\bar{\zeta} - 1/4}$ as defined in equation (A.14). Note that equation (A.33) is more accurate than equations (6) and (7) of [12]. At the polar angle $\theta = \alpha$, the continuity of the radial electric field in equation (12) yields the boundary condition

$$\frac{1}{\varepsilon_m \sin\theta} \frac{\partial}{\partial\theta} \bar{\Psi}(\theta) \sin\theta \bigg|_{\theta\to\alpha-} = \frac{1}{\varepsilon_d \sin\theta} \frac{\partial}{\partial\theta} \bar{\Psi}(\theta) \sin\theta \bigg|_{\theta\to\alpha+} \tag{A.34}$$

or

$$\frac{1}{\varepsilon_m} \left[-\sin\alpha \frac{P'^1_{-(1/2)+\mathrm{i}\nu}(\cos\alpha)}{P^1_{-(1/2)+\mathrm{i}\nu}(\cos\alpha)} + \cot\alpha \right] = \frac{1}{\varepsilon_d} \left[\sin\alpha \frac{P'^1_{-(1/2)+\mathrm{i}\nu}(-\cos\alpha)}{P^1_{-(1/2)+\mathrm{i}\nu}(-\cos\alpha)} + \cot\alpha \right], \tag{A.35}$$

which is equal to the limit of equation (55) as $r \to 0$. Equation (A.35) is also more accurate than equation (16) of [12].

Appendix B. Proof that $F(\theta, r) \to 0$ as $\theta \to \alpha$ for $\Psi(\theta, r) = g(\theta, r)/g(\alpha, r)$ in the extended polar angle equation (9)

The term $F(\theta, r)$ in equation (10) is

$$F(\theta, r) = r^2 \frac{\partial^2 \Psi(\theta, r)}{\partial r^2} + 2r \left(1 + \frac{r}{R(r)} \frac{\partial R(r)}{\partial r} \right) \frac{\partial \Psi(\theta, r)}{\partial r}. \tag{B.1}$$

If the extended angular function $\Psi(\theta, r)$ is symbolically expressed by

$$\Psi(\theta, r) = \frac{g(\theta, r)}{g(\alpha, r)}, \tag{B.2}$$

we have

$$\frac{\partial}{\partial r}\Psi(\theta, r) = \frac{1}{(g(\alpha, r))^2} \left(\frac{\partial g(\theta, r)}{\partial r} g(\alpha, r) - g(\theta, r) \frac{\partial g(\alpha, r)}{\partial r} \right) \tag{B.3}$$

$$\begin{aligned} \frac{\partial^2}{\partial r^2}\Psi(\theta, r) = {} & \frac{1}{(g(\alpha, r))^2} \left(\frac{\partial^2 g(\theta, r)}{\partial r^2} g(\alpha, r) - g(\theta, r) \frac{\partial^2 g(\alpha, r)}{\partial r^2} \right) \\ & - \frac{2}{g(\alpha, r)} \frac{\partial g(\alpha, r)}{\partial r} \frac{\partial}{\partial r} \Psi(\theta, r) \end{aligned} \tag{B.4}$$

which easily leads to

$$\frac{\partial \Psi(\theta, r)}{\partial r} \to 0, \qquad \frac{\partial^2 \Psi(\theta, r)}{\partial r^2} \to 0 \qquad \text{as} \qquad \theta \to \alpha. \tag{B.5}$$

Substituting equation (B.5) into equation (B.1), we obtain $F(\theta, r) \to 0$ as $\theta \to \alpha$ and find that the original equation (9) becomes equivalent to the zeroth-order equation (44) when $\Psi(\theta, r)$ is described as equation (B.2). This means the zeroth-order extended polar angle equation (44) gives an exact solution at the conical surface $\theta = \alpha$ and therefore provides a closely approximate solution around it.

Appendix C. Proof that equation (51) approaches equation (21) as $r \to \infty$ at $\theta \approx \alpha$

A useful formula for the Legendre functions of complex degree [32, 36] is

$$P_{-(1/2)+\mathrm{i}\tau_j(r)}(\cos\theta) \approx \frac{\exp(\tau_j(r)\theta)}{\sqrt{2\pi\,\tau_j(r)\sin\theta}}, \qquad j = m, d \qquad \text{for} \quad \tau_j(r) \to \infty, \tag{C.1}$$

which is applied to the associated Legendre functions

$$P^1_{-(1/2)+\mathrm{i}\tau_j(r)}(\cos\theta) = -(1-\cos^2\theta)^{1/2}\frac{d}{d(\cos\theta)}P_{-(1/2)+i\tau_j(r)}(\cos\theta) \tag{C.2}$$

and hence we find that

$$P^1_{-(1/2)+\mathrm{i}\tau_j(r)}(\cos\theta) \approx \sqrt{\frac{\tau_j(r)}{2\pi\sin\theta}}\exp(\tau_j(r)\theta), \qquad j = m, d \qquad \text{for} \quad \tau_j(r) \to \infty. \tag{C.3}$$

Replacing θ by $\pi - \theta$ in equation (C.3), we obtain

$$P^1_{-(1/2)+\mathrm{i}\tau_j(r)}(-\cos\theta) \approx \sqrt{\frac{\tau_j(r)}{2\pi\sin\theta}}\exp(\tau_j(r)(\pi-\theta)), \quad j = m, d \qquad \text{for} \quad \tau_j(r) \to \infty. \tag{C.4}$$

Substituting equations (C.3) and (C.4) into equation (51), we find that

$$\Psi(\theta, r) = \sqrt{\frac{\sin\alpha}{\sin\theta}}\begin{cases}\exp(\tau_m(r)(\theta-\alpha)), & \theta \leqslant \alpha\\ \exp(\tau_d(r)(\alpha-\theta)), & \theta \geqslant \alpha\end{cases} \qquad \text{for} \quad \tau_j(r) \to \infty, \quad j = m, d. \tag{C.5}$$

From equations (50) and (34), we find that the condition $\tau_j(r) \to \infty$ in equation (C.5) can be replaced by $r \to \infty$. After making the substitution

$$\frac{\sin\alpha}{\sin\theta} \approx 1 \qquad \text{for} \quad \theta \approx \alpha \tag{C.6}$$

and

$$\tau_j(r) \to \beta_j r, \qquad j = m, d \qquad \text{for} \quad r \to \infty, \tag{C.7}$$

equation (C.5) gives the asymptotic representation of $\Psi(\theta, r)$as follows:

$$\Psi(\theta, r) \approx \begin{cases}\exp(\beta_m r(\theta-\alpha)), & \theta \leqslant \alpha\\ \exp(\beta_d r(\alpha-\theta)), & \theta \geqslant \alpha\end{cases} \qquad \text{for} \quad r \to \infty \quad \text{and} \quad \theta \approx \alpha, \tag{C.8}$$

which eventually leads to equation (21).

Appendix D. Approximate behavior of $\zeta^{(0)}(r)$ for small and large r

Figures 3 and 4 show that $\zeta^{(0)}(r)$ becomes larger with smaller cone angle 2α, and hence we consider the boundary condition (55) for $\alpha \ll 1$ and $\zeta^{(0)}(r) \gg 1$. From (C.3), we obtain for $\zeta^{(0)}(r) \gg 1$ that

$$P^1_{-(1/2)+\mathrm{i}\tau_m(r)}(\cos\theta) \approx \sqrt{\frac{\tau_m(r)}{2\pi\sin\theta}}\exp(\tau_m(r)\theta), \tag{D.1}$$

$$P'^1_{-(1/2)+\mathrm{i}\tau_m(r)}(\cos\theta) = \frac{\partial P^1_{-(1/2)+\mathrm{i}\tau_m(r)}(\cos\theta)}{\partial(\cos\theta)} \approx -\frac{\tau_m(r)}{\sin\theta}\sqrt{\frac{\tau_m(r)}{2\pi\sin\theta}}\exp(\tau_m(r)\theta). \tag{D.2}$$

From (C.4), we obtain for $\zeta^{(0)}(r) \gg 1$ that

$$P^{1}_{-(1/2)+\mathrm{i}\tau_d(r)}(-\cos\theta) \approx \sqrt{\frac{\tau_d(r)}{2\pi\sin\theta}}\exp(\tau_d(r)(\pi-\theta)), \tag{D.3}$$

$$P'^{1}_{-(1/2)+\mathrm{i}\tau_d(r)}(-\cos\theta) \approx -\frac{\tau_d(r)}{\sin\theta}\sqrt{\frac{\tau_d(r)}{2\pi\sin\theta}}\exp(\tau_d(r)(\pi-\theta)). \tag{D.4}$$

Substituting equations (D.1)–(D.4) into the boundary condition (55), and using $\alpha \ll 1$, we find that

$$\frac{1}{\varepsilon_m}\left[\tau_m(r)+\frac{1}{\alpha}\right]-\frac{1}{\varepsilon_d}\left[-\tau_d(r)+\frac{1}{\alpha}\right]\approx 0. \tag{D.5}$$

Then, substituting equation (50) into equation (D.5) and rearranging terms, we have

$$\frac{\sqrt{(\beta_m r)^2+\zeta^{(0)}(r)-1/4}}{\varepsilon_m}+\frac{\sqrt{(\beta_d r)^2+\zeta^{(0)}(r)-1/4}}{\varepsilon_d}+\frac{1}{\alpha}\left(\frac{1}{\varepsilon_m}-\frac{1}{\varepsilon_d}\right)\approx 0, \tag{D.6}$$

which is considered for small and large r.

In the case of small r, as $r \to 0$, equation (D.6) approaches

$$\frac{\sqrt{\zeta^{(0)}(0)-1/4}}{\varepsilon_m}+\frac{\sqrt{\zeta^{(0)}(0)-1/4}}{\varepsilon_d}+\frac{1}{\alpha}\left(\frac{1}{\varepsilon_m}-\frac{1}{\varepsilon_d}\right)\approx 0, \tag{D.7}$$

so that

$$\zeta^{(0)}(0) \approx \frac{1}{\alpha^2}\left(\frac{\varepsilon_m-\varepsilon_d}{\varepsilon_m+\varepsilon_d}\right)^2+\frac{1}{4}. \tag{D.8}$$

From equations (D.6) and (D.7), we have

$$\frac{\sqrt{(\beta_m r)^2+\zeta^{(0)}(r)-1/4}-\sqrt{\zeta^{(0)}(0)-1/4}}{\varepsilon_m} + \frac{\sqrt{(\beta_d r)^2+\zeta^{(0)}(r)-1/4}-\sqrt{\zeta^{(0)}(0)-1/4}}{\varepsilon_d}\approx 0. \tag{D.9}$$

To approximately estimate equation (D.9), using the approximation

$$(1+x)^{1/2}-1 \approx \tfrac{1}{2}x \qquad \text{for} \quad |x| \ll 1, \tag{D.10}$$

we have for small r that

$$\frac{(\beta_m r)^2+\zeta^{(0)}(r)-\zeta^{(0)}(0)}{\varepsilon_m}+\frac{(\beta_d r)^2+\zeta^{(0)}(r)-\zeta^{(0)}(0)}{\varepsilon_d}\approx 0. \tag{D.11}$$

Finally, we obtain

$$\zeta^{(0)}(r) \approx \zeta^{(0)}(0)+k_p^2 r^2 \qquad \text{for} \quad \frac{r}{\lambda_0} \ll \frac{1}{2\sqrt{2}\pi\alpha}, \tag{D.12}$$

which shows a square increase around $r = 0$.

In the case of large r, translating equation (D.6) into the form

$$\frac{\beta_m r\sqrt{1+\{\zeta^{(0)}(r)-1/4\}/(\beta_m r)^2}}{\varepsilon_m}+\frac{\beta_d r\sqrt{1+\{\zeta^{(0)}(r)-1/4\}/(\beta_d r)^2}}{\varepsilon_d}+\frac{1}{\alpha}\left(\frac{1}{\varepsilon_m}-\frac{1}{\varepsilon_d}\right)\approx 0 \tag{D.13}$$

and applying equation (D.10) to equation (D.13), we have

$$\frac{\beta_m r\left(1+\frac{1}{2}\{\zeta^{(0)}(r)-1/4\}/(\beta_m r)^2\right)}{\varepsilon_m}+\frac{\beta_d r\left(1+\frac{1}{2}\{\zeta^{(0)}(r)-1/4\}/(\beta_d r)^2\right)}{\varepsilon_d}$$
$$+\frac{1}{\alpha}\left(\frac{1}{\varepsilon_m}-\frac{1}{\varepsilon_d}\right)\approx 0 \tag{D.14}$$

or

$$\frac{\zeta^{(0)}(r)-1/4}{2\varepsilon_m\beta_m r}+\frac{\zeta^{(0)}(r)-1/4}{2\varepsilon_d\beta_d r}+\frac{1}{\alpha}\left(\frac{1}{\varepsilon_m}-\frac{1}{\varepsilon_d}\right)\approx 0. \tag{D.15}$$

Finally, we obtain

$$\zeta^{(0)}(r)\approx\frac{2\beta_m\beta_d}{\alpha}\left(\frac{\varepsilon_m-\varepsilon_d}{\varepsilon_m\beta_m-\varepsilon_d\beta_d}\right)r \qquad \text{for} \quad \frac{r}{\lambda_0}\gg\frac{1}{\pi\alpha\sqrt{|\varepsilon_m|}}. \tag{D.16}$$

We can summarize by saying that the approximate behaviors of $\zeta^{(0)}(r)$ for small and large r show a square increase such as in equation (D.12) and a linear increase such as in equation (D.16), respectively. Comparing these approximate behaviors with equations (56)–(59), we obtain roughly approximate relations as follows:

$$\zeta^{(0)}(0)\approx\frac{1}{\alpha^2}\left(\frac{\varepsilon_m-\varepsilon_d}{\varepsilon_m+\varepsilon_d}\right)^2+\frac{1}{4} \tag{D.17}$$

$$a\approx k_p^2 \tag{D.18}$$

$$p\approx\frac{2}{\alpha}\left(\frac{\varepsilon_m-\varepsilon_d}{\varepsilon_m\beta_m-\varepsilon_d\beta_d}\right) \tag{D.19}$$

$$q=\frac{p}{2a}\approx\frac{1}{\alpha k_p^2}\left(\frac{\varepsilon_m-\varepsilon_d}{\varepsilon_m\beta_m-\varepsilon_d\beta_d}\right). \tag{D.20}$$

References

[1] Stockman M I 2004 Nanofocusing of optical energy in tapered plasmonic waveguides *Phys. Rev. Lett.* **93** 137404
[2] Bouhelier A, Renger J, Beversluis and Novotony 2003 Plasmon-coupled tip-enhanced near-field optical microscopy *J. Microsc.* **210** 220
[3] Keilmann F 1999 Surface-polariton propagation for scanning near-field optical microscopy application *J. Microsc.* **194** 567
[4] Kawata S 2001 *Near-Field Optics and Surface Plasmon Polaritons* (Berlin: Springer)
[5] Srituravanich W, Fang N, Sun C, Luo Q and Zhang X 2004 Plasmonic nanolithography *Nano Lett.* **4** 1085
[6] Liu Z-W, Wei Q-G and Zhang X 2005 Surface plasmon interference nanolithography *Nano Lett.* **5** 957
[7] Kneipp K, Wang Y, Kneipp H, Perelman L T, Itzkan I, Dasari R R and Feld M S 1997 Single molecule detection using surface-enhanced Raman scattering (SERS) *Phys. Rev. Lett.* **78** 1667
[8] Nie S and Emory S R 1997 Probing single molecules and single nanoparticles by surface-enhanced Raman scattering *Science* **275** 1102
[9] Hartschuh A, Pedrosa H N, Novotny and Krauss T D 2003 Simultaneous fluorescence and Raman scattering from single carbon nanotubes *Science* **301** 1354
[10] Pettinger B, Ren B, Picardi G, Schuster R and Ertl G 2004 Nanoscale probing of adsorbed species by tip-enhanced Raman spectroscopy *Phys. Rev. Lett.* **92** 096101
[11] Ichimaru T, Hayazawa N, Hashimoto M, Inouye Y and Kawata S 2004 Tip-enhanced coherent anti-Stokes Raman scattering for vibrational nanoimaging *Phys. Rev. Lett.* **92** 220801
[12] Babadjanyan A J, Margaryan N L and Nerkarayan Kh V 2000 Superfocusing of surface polaritons in the conical structure *J. Appl. Phys.* **87** 3785
[13] Ruppin R 2005 Effect of non-locality on nanofocusing of surface plasmon field intensity in a conical tip *Phys. Lett.* A **340** 299

[14] Denk W and Pohl D W 1991 Near-field optics: microscopy with nanometer-size fields *J. Vac. Sci. Technol.* B **9** 510
[15] Nerkarayan Kh V 1997 Superfocusing of a surface polariton in a wedge-like structure *Phys. Lett.* A **237** 103
[16] Smolyaninov I I, Balzano Q and Davis C C 2005 Plasmon-polaritons on the surface of a pseudosphere *Phys. Rev.* B **72** 165412
[17] Gramotonev D K 2005 Adiabatic nanofocusing of plasmons by sharp metallic grooves: geometrical optics approach *J. Appl. Phys.* **98** 104302
[18] Pile D F P 2006 Adiabatic and nonadiabatic nanofocusing of plasmons by tapered gap plasmon waveguides *Appl. Phys. Lett.* **89** 041111
[19] Gurevich V S and Libenson M N 1995 Surface polaritons propagation along micropipettes *Ultramicroscopy* **57** 277
[20] Devaux E, Dereux A, Bourillot E, Weeber J-C, Lacroute Y and Goudonnet J-P 2000 Local detection of the optical magnetic field in the near zone of dielectric samples *Phys. Rev.* B **62** 10504
[21] Schröter U and Dereux A 2001 Surface plasmon polaritons on metal cylinders with dielectric core *Phys. Rev.* B **64** 125420
[22] Taflove A and Hagness S C 2005 *Computational Electrodynamics: The Finite-Difference Time-Domain Method* 3rd edn Norwood Artech House Publishers)
[23] Polyanin A D 2001 *Handbook of Linear Partial Differential Equations for Engineers and Scientists* (Boca Raton, FL: Chapman and Hall/CRC Press)
[24] Polyanin A D and Zaitsev V F 2003 *Handbook of Nonlinear Partial Differential Equations* (Boca Raton, FL: Chapman and Hall/CRC Press)
[25] Polyanin A D and Manzhirov A V 2006 *Handbook of Mathematics for Engineers and Scientists* (Boca Raton, FL: Chapman and Hall/CRC Press)
[26] Sommerfeld A 1912 Die Greensche Functionen der Schwingungsgleichung *Jahresber. Deutch. Math. Verein.* **21** 309
[27] Born M and Oppenheimer J 1927 Zur Quantentheorie der Molekeln *Ann. Phys.* **84** 457
[28] Born M and Huang K 1954 *Dynamical Theory of Crystal Lattices* (London: Oxford University Press)
[29] Jackson J D 1998 *Classical Electrodynamics* 3rd edn (Hoboken: Wiley)
[30] Samble J R, Bradbery G W and Yang F 1991 Optical excitation of surface plasmons: an introduction *Contemp. Phys.* **32** 173
[31] Farlow S J 1993 *Partial Differential Equations for Scientists and Engineers* (New York: Dover)
[32] Lebedev N N 1972 *Special Functions and their Applications* (New York: Dover)
[33] Abramowitz M and Stegun I A 1972 *Handbook of Mathematical Functions with Formulas, Graphs, and Mathematical Tables* 9th edn (New York: Dover)
[34] Innes R A and Sambles J R 1987 Optical characterization of gold using surface plasmon-polaritons *J. Phys. F: Met. Phys.* **17** 277
[35] Dunster T M 1990 Bessel functions of purely imaginary order, with an application to second-order linear differential equations having a large parameter *SIAM J. Math. Anal.* **21** 995
[36] Olver F W J 1997 *Asymptotics and Special Functions* (Natick: A K Peters, Ltd.)